

Longitudinal vortices in unsteady Taylor–Couette flow: solution to a 60-year-old mystery

Ashley P. Willis¹† and Michael J. Burin²

¹Applied Mathematics, School of Mathematical and Physical Sciences, Hicks Building, University of Sheffield, Sheffield S3 7RH, UK

²Department of Physics, California State University, San Marcos, California 92096 USA

(March 2025)

Applying a sufficiently rapid start-stop to the outer cylinder of the Couette–Taylor system, structures approximately aligned with the axis were recorded in the classic work of Coles (1965). These short-lived rolls are oriented perpendicular to the classic Taylor-vortex rolls. In this work we report numerical observation of this instability, guided by a more recent experimental observation. The instability is shown to be related to an inflection in the azimuthal velocity profile, a finding consistent with the experimental observations of its emergence during the deceleration phase. Despite the transient nature of start-stop experiments, we show that the instability can be linked to that of the oscillating boundary layer problem of Stokes. There are several reasons why the instability may have remained elusive, both for experimental observation and intrinsic to the idealized system. We look in more detail at dependence on the radius ratio for the Taylor–Couette system and find that, in the case where the size of the rolls scales with the gap width, for radius ratios any lower than that used by Coles, $R_i/R_o = 0.874$, the instability is quickly overrun by axisymmetric rolls of Görtler type.

1. Introduction

The nature of the flow of fluid between two rotating cylinders has long played a special role in the study of fluid dynamics and dynamical systems. Taylor (1923) demonstrated that linear stability analysis, using the no-slip condition, could accurately predict the onset of rolls. A large number of distinct flow regimes were soon identified, and Coles (1965)(figure 2 therein) created a summary graphic in the plane defined by the rotation rates of the inner and outer cylinders. This plot included Taylor’s original stability line, above which greater rotation of the inner cylinder rendered the flow unstable to the ‘singly periodic flow’ (Taylor-vortices), and catalogued regions of ‘doubly periodic flow’ (wavy Taylor-vortices), spiral and turbulent flows. Coles was particularly interested in the multiplicity of wavy Taylor vortex states, of various azimuthal wavenumber, and transitions between them. A celebrated version of this diagram, including a greater range of flows, was produced by Andereck *et al.* (1986). It is

† Email address for correspondence: a.p.willis@sheffield.ac.uk

now a little over 100 years since Taylor’s landmark paper, 60 years since the classic work of Coles, and the rich dynamical landscape of the Taylor–Couette flow, for the steady rotating case alone, is well recognised.

Multiple flow states for the same rotation rates are not easily represented on a summary graphic, and figure 8 of Coles (1965) a recognised example of this complexity. The addition of time-dependence likewise introduces an extra dimension of complexity, and expeditions in these directions are fewer but significant. Görtler rolls arise appear when flow encounters a curved surface, and like Taylor-vortex rolls, they are aligned with the direction of the flow and caused by a centrifugal instability. Görtler rolls have been observed to form and eventually evolve into Taylor-vortices for the case of an impulsive start of the inner cylinder, see e.g. Neitzel *et al.* (1995). Studies of an impulsive stop for the outer cylinder include Kohuth & Neitzel (1988); Verschoof *et al.* (2016); Ostilla-Mónico *et al.* (2017); Singh & Prigent (2021), where rolls of many sizes appear and decay, leaving behind the largest. Periodic modulations of the rotation rate of either cylinder have been studied, e.g. Ern & Wesfreid (1999) found regimes of both destabilisation and stabilisation, Youd *et al.* (2003) observed that Taylor-vortex rolls may or may-not reverse the direction of the roll, and Verschoof *et al.* (2018) examined the effect of modulations on turbulent flows at high Reynolds numbers. In the context of planetary libration, an interesting set of experiments and calculations with modulated rotation rates have been performed, e.g. Noir *et al.* (2010); Lopez & Marques (2011). Axial oscillations of the inner cylinder have been shown to suppress Taylor instability by Marques & Lopez (1997). All these cases, however, typically manifest the same instabilities, i.e. the appearance of modified Taylor-vortices or Görtler rolls.

1.1. *Experimental observations of longitudinal vortices*

Coles (1965) includes an image, figure 22(o) therein and reproduced in figure 1 (*left*) here, that appears unlike any of the flows mentioned above. While those flows are dominated by azimuthally aligned rolls that wrap around the cylinder, here the waves are aligned with the axis. In a footnote (p410), Coles describes his method for establishing wavy Taylor vortex flow with a high ‘tangential’ wavenumber, now more commonly referred to as the azimuthal wavenumber m : “*The usual experimental method for establishing a flow with a high tangential wavenumber was to approach the final operating condition from the singly-periodic side [from axisymmetric Taylor rolls] with two cylinders initially rotating in the same direction. A sufficiently fast stop for the outer cylinder then usually led to a flow with a large number of tangential waves, probably as a result of Tollmein instability in the unsteady viscous layer on the wall of the outer cylinder (cf. figure 22(o), plate 12).*” The Tollmein–Schlichting instability is a viscous instability that can occur in a boundary layer flow, such as when a unidirectional flow encounters a flat plate. The rolls that arise within the boundary layer are aligned spanwise to the direction of the flow. In principle, it is possible the sudden-stop could indeed set up a boundary-layer type flow and hence Tollmein instability. However, Coles’ caption to figure 22(o) reads only “*(o) Instability following start-stop motion of outer cylinder.*” The sudden-stop and start-stop experiments are potentially quite different! Unfortunately, no parameters for the start-stop experiment were provided.

More recently, during an experimental campaign to characterize turbulence driven by outer cylinder motion (Burin & Czarnocki 2012), a brief set of start-stop observations were made, revealing what appears to be the same azimuthal instability as described above. See figure 1 (b). The instability in this experiment was observed to arise during the decelerating phase, and for only a narrow gap width ($d = 6.3$ mm and radius ratio $R_i/R_o = 0.97$), although its apparent absence for wider gap widths could be due to visualization shortcomings. A qualitative dependence of the instability wavelength with respect to forcing was observed, with initial acceleration provided by falling weights coupled to the drive system, while

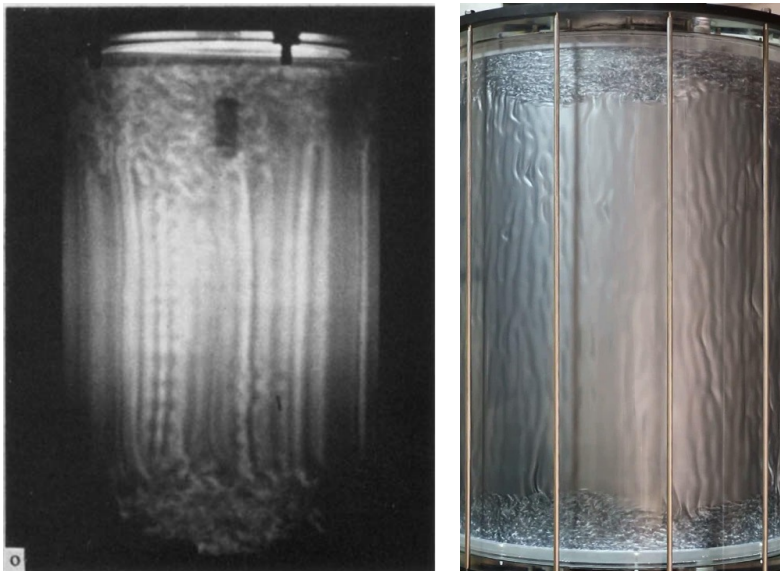


Figure 1: (left) Figure 22(o) of Coles (1965), captioned ‘Instability following start-stop motion of outer cylinder.’ (right) Similar observation from the experiments of Burin & Czarnocki (2012)

mechanical friction provided deceleration. As the acceleration increased, the wavelength increased by a factor of two: from 1.3 to 2.5 cm, or (approximately) 2 to 4 gap widths. For smaller accelerations the instability was not seen, and for higher ones the turbulence emanating from the end-caps engulfed the central region before the instability could presumably appear.

To our knowledge, there has been no systematic study of this transitory TC flow state. In this paper, using new simulations alongside these scarce laboratory observations, we aim to clarify when the longitudinal vortices should appear, with respect to the type of motion of the outer cylinder, and to identify the instability mechanism. We show how this particular unsteady flow may be understood within the wider context of unsteady boundary flows, along the way linking Taylor–Couette flow to a branch of fluid mechanics reaching back to Stokes’ oscillating boundary layer problem.

2. Methods

We consider the flow between concentric cylinders of radius R_i and R_o , where the subscripts indicate the inner and outer cylinders respectively, with rotation rates Ω_i and Ω_o . The radius ratio is denoted by $\eta = R_i/R_o$ and gap width $d = R_o - R_i$. Scales used in the non-dimensionalisation of the governing equations are the gap width d and the viscous diffusion timescale d^2/ν , where ν is the kinematic viscosity, which combine to give a velocity scale ν/d . Quantities in all figures are non-dimensionalised with these scales.

The dimensionless Navier–Stokes equations are

$$\partial_t \mathbf{u} + \mathbf{u} \cdot \nabla \mathbf{u} = -\nabla p + \nabla^2 \mathbf{u}, \quad \nabla \cdot \mathbf{u} = 0. \quad (2.1)$$

Note that the Reynolds numbers, $Re_{i,o} = R_{i,o}\Omega_{i,o}d/\nu$, do not appear in the governing equation but determine the speed of the boundaries: $u_\theta = Re_i$ at $r_i = \eta/(1-\eta)$ and $u_\theta = Re_o$ at $r_o = r_i + 1$.

When $Re_{i,o}$ are constant, steady circular-Couette flow is given by

$$\mathbf{u} = V_0(r)\hat{\boldsymbol{\theta}}, \quad V_0(r) = \frac{1}{1+\eta} \left[(Re_o - \eta Re_i)r + \frac{\eta}{(1-\eta)^2} (Re_i - \eta Re_o) \frac{1}{r} \right]. \quad (2.2)$$

To implement the case when time-dependent $\Omega_{i,o}(t)$ imply time-dependent $Re_{i,o}(t)$, we consider the deviation \mathbf{u}' of the velocity field from (2.2) evaluated at each instant, $V_0(r, t) = V_0(r; Re_i(t), Re_o(t))$, i.e.

$$\mathbf{u}(\mathbf{x}, t) = V_0(r, t)\hat{\boldsymbol{\theta}} + \mathbf{u}'(\mathbf{x}, t). \quad (2.3)$$

The field $V_0(r, t)$ is used only in the computations and should be distinguished from the ‘mean profile’ $V(r, t)$, which denotes the θ - and z -average of the flow \mathbf{u} . The governing equation for \mathbf{u}' can then be written

$$(\partial_t - \nabla^2)\mathbf{u}' = \mathbf{u} \times (\nabla \times \mathbf{u}) - \nabla p - (\partial_t V_0)\hat{\boldsymbol{\theta}}, \quad (2.4)$$

subject to $\nabla \cdot \mathbf{u}' = 0$ with boundary conditions $\mathbf{u}' = \mathbf{0}$ at $r = r_{i,o}$. The code used for time integration of (2.4) is a long-standing variant of the *Openpipeflow* solver (Willis 2017), and modification for this case required only the addition of the forcing term, i.e. the known last term on the right-hand side of (2.4). Periodicity is assumed in the axial dimension over a length $2\pi/\alpha$, and m -fold periodicity can be imposed in the azimuthal dimension. Variables are discretised in the form

$$a(r_n, \theta, z) = \sum_{|k| < K} \sum_{|m'| < M} A_{km}(r_n) e^{i(\alpha kz + m m' \theta)}, \quad n = 1, \dots, N. \quad (2.5)$$

$N = 100$ for most calculations, while, for linear stability calculations, K and M are only as large as required to capture the first few modes. The Crank–Nicolson method is applied to the diffusion term, while an Euler–predictor and Crank–Nicolson corrector are applied the first and last terms on the right-hand side of (2.4). Via the pressure–Poisson equation, p is used to project the velocity onto the space of divergence-free functions, using an influence-matrix technique to implement the no-slip and divergence-free condition at the wall simultaneously. The difference between the predictor and corrector may be used to control the timestep, but for the calculations here, the timestep is fixed at $\Delta t = 10^{-6}$. (Note that the dimensionless advective timescale $1/|\mathbf{u}| \sim 1/Re_o$.)

The mean profile (θ, z -average) is the component $V(r, t) = u'_{\theta,00} + V_0(r, t)$, where the subscript 00 indicates the $k = m' = 0$ mode in (2.5). In the absence of perturbations, the mean profile is quickly computed by simulating with $K = M = 1$. Eigenvalues, which give the growth rates of linear perturbations to the base flow, are calculated by combining time-integration with Arnoldi iteration, which enables capture of more than just the leading mode.

3. Results

3.1. Approximation of experiment

The inner cylinder is fixed, $Re_i = 0$, and supposing that instability in the preliminary experiment was excited by an approximately constant acceleration and deceleration, we begin with a linear ramp up and down in the Reynolds number for the outer cylinder:

$$Re_o(t) = \begin{cases} U_1 t/T_1, & 0 \leq t < T_1, \\ U_1 (T_2 - t)/(T_2 - T_1), & T_1 \leq t < T_2, \\ 0, & T_2 \leq t. \end{cases} \quad (3.1)$$

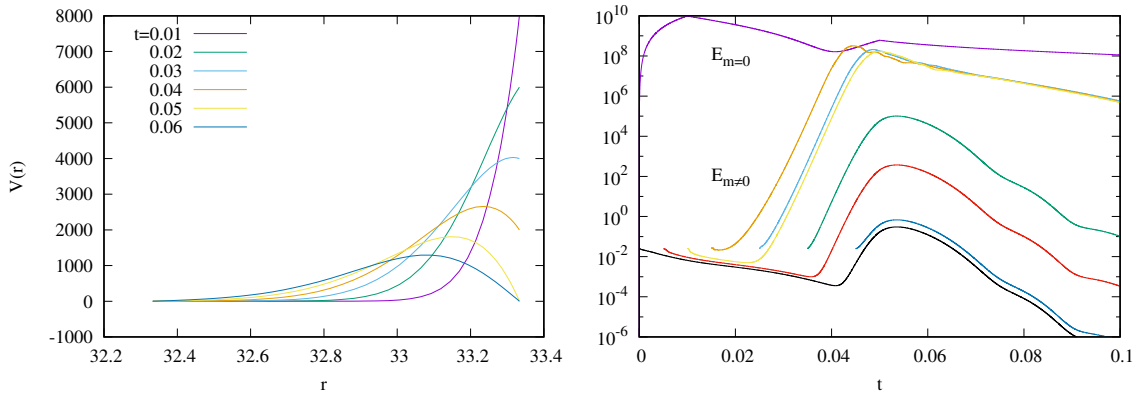


Figure 2: (left) Mean profile during the ramp up and ramp down of the outer cylinder velocity. (right) Energy of the mean flow $E_{m=0}$, and energy of perturbations $E_{m \neq 0}$ ($\lambda \approx 3.5$) introduced at various times.

Inspection of videos of the experiments for the narrow gap case, $\eta = 0.97$, suggested that instability with an azimuthal wavelength $\lambda \approx 3.5$ (gap widths) should be observable with dimensionless parameters $U_1 = 8000$, $T_1 = 0.01$, $T_2 = 0.05$. Using $\lambda \approx 2\pi r_o/m$, where $r_o = 1/(1 - \eta)$ and m is the rotational symmetry (see (2.5)), implied setting $m = 60$.

Figure 2(left) shows calculations of the azimuthal mean flow profile $V(r, t)$ during the ramp up and ramp down of the outer cylinder. Perturbations to the velocity are added to $V(r, t)$ that are very small, so that the Fourier modes of the perturbation may be considered to be linearly independent. As the rolls to be identified are axially aligned, we consider only modes with $k = 0$ in (2.5) so that the calculations are two-dimensional (axially-independent). Small perturbations are added for m' up to 7, but the $m' = 1$ mode is always found to be dominant. Figure 2(right) shows time series of the energy summed over all azimuthally-dependent ($m' \neq 0$) perturbations. It was found that perturbations added at $t = 0$ would not grow substantially. Instead, perturbations added at later times during the development of the mean profile were necessary to trigger transient instability. (In the physical experiment, it is perhaps reasonable that some noise is always present, from end conditions at least.) Growth rates appear to be approximately constant for times 0.02-0.04, which is during the decelerating phase, consistent with the appearance of the instability in the experiment.

It is possible in our numerical calculations to freeze the mean profile $V(r, t)$ at a particular time and to calculate the growth rates of infinitesimal disturbances. For this to produce physically reasonable growth rates, it assumes that there is time for the disturbances to grow substantially more rapidly than changes in the base profile. In figure 2(right), it is seen that perturbations can grow many orders of magnitude in a short time. With this frozen profile assumption, figure 3(left) shows the growth rates of perturbations to the profile as a function of azimuthal wavelength λ at several times. Peak growth is observed at $t = 0.04$ for a wavelength of $\lambda \approx 2.5$, but observe that instability starts earlier at longer wavelengths, $\lambda \approx 3$ for $t = 0.02$ (approximately when growth is first observed), which is a reasonable match to the wavelength observed in the experiment.

For the purely azimuthal base flow $\mathbf{u} = V(r, t)\hat{\theta}$, the nonlinear terms in (2.1) are zero, so that \mathbf{u} can be multiplied through by an arbitrary constant and remains a solution. Therefore, if U_1 is changed without altering T_1 and T_2 , the mean flow is multiplied by a factor but does not change structure. Looking at the time $t = 0.04$ where growth was maximised, figure 3(right) shows that a change in amplitude of the start-stop changes the growth rate of perturbations, but has no noticeable effect on the preferred wavelength of instability.

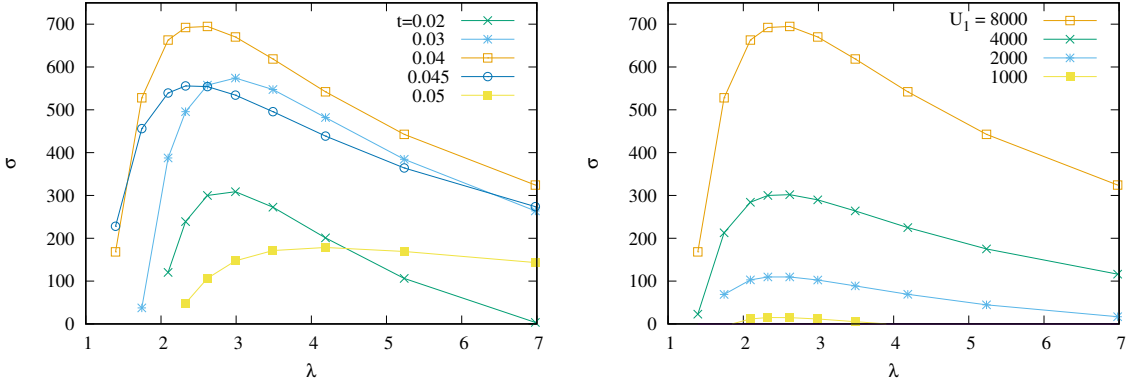


Figure 3: (*left*) Growth rates as a function of azimuthal wavelength λ , assuming frozen mean profiles at the given times. $U_1 = 8000$, $T_1 = 0.01$, $T_2 = 0.05$. (*right*) Growth rates at $t = 0.04$ changing only U_1 .

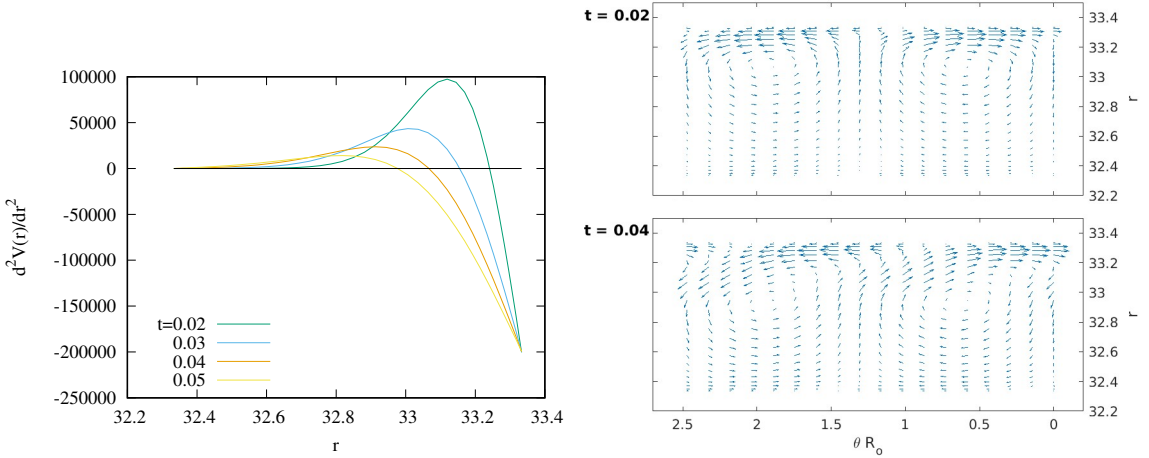


Figure 4: (*left*) Second derivative of the mean profile – roots indicate the location of an inflection point. (*right*) Eigenfunctions of the leading unstable mode with $\lambda \approx 2.6$ at the given times.

In the Introduction, it was noted that Coles (1965) had postulated that the rolls ‘probably’ appeared as the result of Tollmein instability, which appears in the boundary layer problem. Acceleration of the boundary sets up a velocity profile of the boundary layer type, but the decelerating phase introduces an inflection point, and it is during this phase that the instability is observed. Figure 4(*left*) shows the second derivative of the mean profiles at several times, so that the zero of this function tracks the position of an inflection point. Using a wavelength $\lambda \approx 2.6$ ($m = 80$), around the value of theoretical preferred wavelength from figure 3, figure 4(*right*) shows eigenfunctions at times 0.02 and 0.04 (as viewed from above, looking down the axis of the cylinders). Although the rolls are not centred precisely on the radial location of the inflection point, they are close and move further from the boundary as t increases. Figure 5 shows the leading growth rates (of modes with strictly m -periodic dependence) as a function of t . At $t = 0$, the mean flow is zero, so all growth rates are associated with

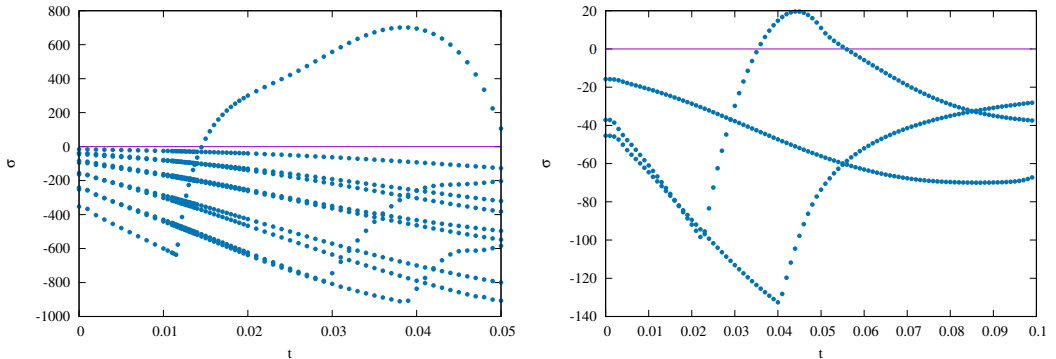


Figure 5: Leading growth rates as a function of t for $\lambda \approx 2.6$ ($m = 80$) at (left) $U_1 = 8000$, $T_1 = 0.01$, $T_2 = 0.05$, and (right) changing only $U_1 = 1000$.

free decay modes. Modes associated with Tollmein instability should arise during the ramp up from $t = 0$ to $t = T_1 = 0.01$, but we only see slow variation of the growth rates of the free-decay modes. From $t = T_1$, deceleration occurs, the inflection is introduced into the mean profile, and the mode associated with the observed longitudinal vortices quickly appears.

3.2. Comparison with Stokes' oscillating boundary problem

Stokes found an analytic solution for the flow induced in a semi-infinite body of fluid by a sinusoidal oscillation of an infinite plate. For a plate moving at (dimensional) speed $U = U_0 \cos(\omega t)$, a viscous length scale may be defined, $\delta = \sqrt{2\nu/\omega}$, which measures the penetration depth of the velocity fluctuations. Scaling with U_0 and δ gives a Reynolds number $R^\delta = U_0\delta/\nu$. Von Kerczek & Davis (1974) considered the linear stability of the base flow at each instant for a channel of width d , where the second wall is stationary. For most calculations, the ratio of scales was $\beta = d/\delta = 8$, for which it was shown that the influence of channel width was negligible. The most dangerous velocity profile was found to be at time $t = \pi/2$ and that rolls of wavenumber $\alpha = 0.5$ first go unstable at $R^\delta = 86$. Blondeaux & Vittori (2021) have more recently revisited this analysis for $\beta \rightarrow \infty$, confirming the results of Von Kerczek & Davis (1974). They also examined for which R^δ there is instability in the accelerating phase or over the whole cycle.

To produce the counterpart instability in the Taylor–Couette apparatus, we suppose that the gap for the channel, $d = \beta\delta$, coincides with the Taylor–Couette gap width d , and expect that correspondence will be best for the narrow gap, where curvature terms are small relative to the viscous terms. For the Taylor–Couette system we put $Re_o = U_1 \sin(2\pi t/T)$.

Converting scales from the channel to Taylor–Couette system, we have $\delta = \sqrt{2\nu/\omega} = \sqrt{2\nu(T(d^2/\nu)/(2\pi))} = d\sqrt{T/\pi}$, then using $\beta = d/\delta$ gives $T = \pi/\beta^2$. Maintaining that $\beta = 8$ for the Taylor–Couette system determines a period for the oscillation $T = \pi/8^2 \approx 0.05$. For the velocity amplitude, $U_1 (\nu/d) = U_0$ implies $U_1 = U_0 d/\nu = (d/\delta)(U_0\delta/\nu) = \beta R^\delta$. The critical $R^\delta = 86$ predicts that the amplitude is critical for $U_1 = 688$. The azimuthal wavenumber is given by $m = 2\pi R_o/\lambda = 2\pi(1/(1-\eta))d/((2\pi/\alpha)\delta)$, which for radius ratio $\eta = 0.97$ and $\beta = 8$ give $m \approx 133$. Using these parameters for the Taylor–Couette setup, figure 6 shows the real part of the three leading growth rates for perturbations to frozen mean profiles. The range in t shown corresponds to half a period, as the mean flow is reversed in the second half and has the same growth rates. (Nine oscillations are simulated first to eliminate

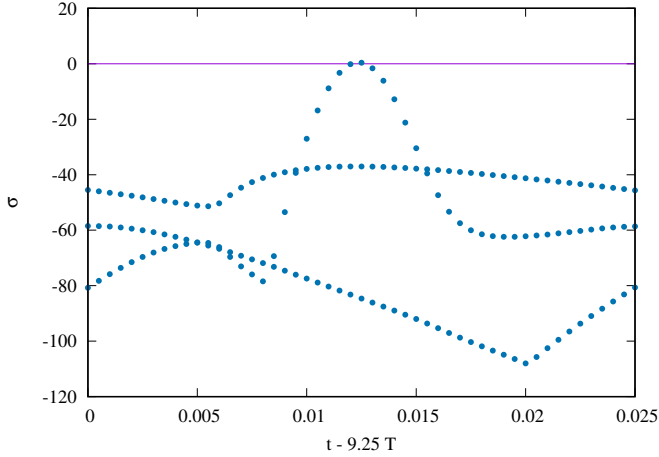


Figure 6: Three leading growth rates for a sinusoidal oscillation of amplitude U_1 in the Taylor-Couette calculation. Parameters for critical U_1 and wavenumber m predicted from Stokes oscillation in a channel. Calculations cover half of the period $T = 0.05$, the base flow is reversed in the second half.

any transient originating from the initial condition $\mathbf{u}' = \mathbf{0}$ at $t = 0$.) The leading growth rate just touches criticality at the expected time in the cycle, indicating that the prediction derived from the channel calculation of Von Kerczek & Davis (1974) is very good.

Qualitatively, the structure of the growth rates in figure 6 is not dissimilar to those of figure 5(right) for the start-stop experiment of §3.1. To make an approximately quantitative link, we make a rough approximation that the linear ramp up and ramp down over a time T_2 corresponds to one half of a sinusoidal oscillation of period $T = 2T_2$. Then, $T = \pi/\beta^2$ for our experiment with $T_2 = 0.05$ implies $\beta = \sqrt{\pi/0.1} \approx 5.6$. This value is not so far from the $\beta = 8$ of Von Kerczek & Davis (1974), suggesting that, if the instability is of the same nature, the result of §3.1 should not have been substantially influenced by the inner boundary. It should then be possible to predict the most unstable wavelength of the instability from that of the Stokes problem. The wavenumber $\alpha = 0.5$ based on units δ for the channel corresponds to an azimuthal wavelength of $\lambda = (2\pi/\alpha)/\beta \approx 2.2$ in gap widths d . In figure 3 it was found that the peak growth rate occurred for $\lambda \approx 2.5$ in the start-stop experiment, a difference of around 10-20%.

3.3. Dependence on radius ratio

In this section we return to the start-stop problem and consider the case where R_o is fixed and R_i decreases, so that the gap d increases and $\eta = R_i/R_o$ decreases.

If $\Omega_o(t)$ is also unchanged, then the penetration depth δ does not change, and $\beta = d/\delta$ increases. It has been confirmed in calculations that the flow near the outer cylinder is independent of the inner cylinder, and there is no change to the instability (therefore not shown).

If d is increased and $\Omega_o(t)$ scaled such that δ increases proportionately, i.e. $\beta = d/\delta$ is held fixed, then wavelength of the instability will continue to scale with d and the wavenumber m decreases. In this case we expect more influence from the curvature. Conveniently, the dimensionless velocity at the boundary, $V(R_o, t)$, and the time-dependent Reynolds number $Re_o(t)$ are unchanged, as our non-dimensionalisation is already based on the viscous time

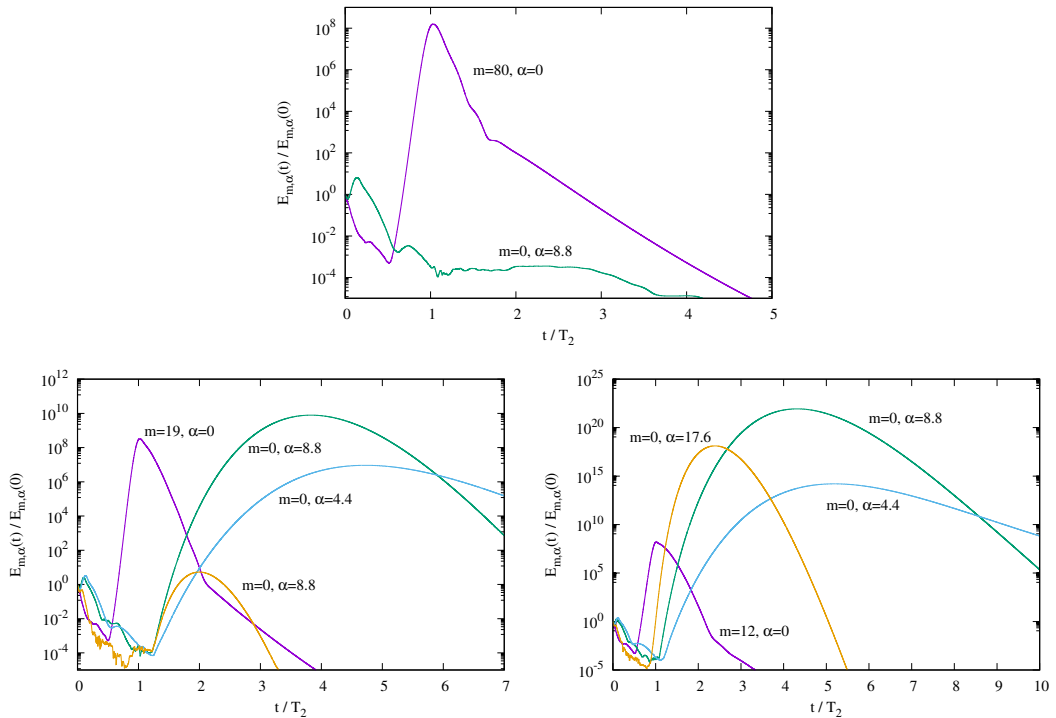


Figure 7: Energy of modes of azimuthal and axial wavenumbers m and α for (top) $\eta = 0.97$, (left) $\eta = 0.874$, (right) $\eta = 0.8$ with start-stop parameters $U_1 = 8000$, $T_1 = 0.01$, $T_2 = 0.05$. For all cases, modes with non-zero m have azimuthal wavelength $\lambda \approx 2.6$.

scale and on d . Only the wavenumber m changes with η : for a change $d \rightarrow \tilde{d}$ and $\eta \rightarrow \tilde{\eta}$, we have $\tilde{m} = m d / \tilde{d} = m (1 - \eta) / (1 - \tilde{\eta})$.

Figure 7 compares the growth of different Fourier modes for $\eta = 0.97, 0.874, 0.8$. The longitudinal vortices are axially independent $\alpha = 0$ and the $m \neq 0$ corresponds to $\lambda \approx 2.6$ for all radius ratios η . The growth of this mode is similar for all cases. For the azimuthally independent mode, $m = 0$, it is guessed that vortices of Görtler type might appear with axial wavelength $2\delta/d = 2/\beta$. For $\beta = 5.6$, this gives axial wavenumber $\alpha = 2.8\pi \approx 8.8$. Such modes do not grow for the narrow gap at $\eta = 0.97$, but for $\eta = 0.8$ they are expected to swamp any trace of the longitudinal vortices in a flash. Interestingly, Coles' choice of $\eta = 0.874$ appears to have been a serendipitous one, close to the borderline where both modes might be observed.

4. Conclusions

The figure 22(o) of Coles (1965), captioned “(o) instability following start-stop motion of the outer cylinder,” with its longitudinal vortices, has been a bit of a longstanding mystery. When Coles described his procedure for introducing different azimuthal wavenumbers m for wavy Taylor-vortex rolls, he mentioned a sudden-stop that induced a large number of waves, “probably as a result of Tollmein instability,” but referred to the image captioned for a start-stop experiment.

In this work, we have simulated the appearance of longitudinal rolls in the Taylor–Couette

system, guided by its unexpected appearance in a more recent experimental campaign (Burin & Czarnocki 2012). We have shown that instability is linked to an inflection point in the mean profile (rather than the Tollmein instability). Despite the transient nature of the start-stop flow, it is possible to link the instability to that of Stokes oscillating boundary problem.

There are a number of reasons why the instability may remain elusive. One, of course, is the rich array of other instabilities exhibited by the system, which create other interesting and more manifest diversions. In the recent experiment, longitudinal vortices were only observed for the case $\eta = 0.97$. Guided by this experiment, our parameters suggested a ratio for the viscous scale δ and the gap d of $\beta = d/\delta \approx 5.6$. From the radial extent of the rolls, seen in figure 4(right), it is expected if β is significantly decreased, then without sufficient physical space for the rolls, the instability will be suppressed.

In our calculations where β is fixed while decreasing the radius ratio, i.e. the rolls scale with the gap width, the radius ratio $\eta = 0.874$ of Coles (1965) appears to be around the lower limit at which the instability might be observable. At lower η , the magnitude of curvature terms raises relative to viscous terms, and the instability is almost immediately swamped by centrifugal instability and the formation of Görtler rolls.

It is less obvious why the instability has not been observed for larger β , where the gap d widens but δ is kept the same. This occurs when R_o and $\Omega_o(t)$ are unchanged and only R_i is reduced. Although the instability should be observable in principle, there are practical challenges, and few, if any, of the experiments we have referenced have been looking in the right regime, combining a start-stop or sinusoidal oscillation with a large Reynolds number. For the traditional case of a stationary outer cylinder and steadily rotating inner cylinder, for $\eta = 0.97, 0.874, 0.8$ the critical Reynolds numbers are respectively $Re_i \approx 239, 118, 95$. Here, for a change $d \rightarrow \tilde{d}$, matching the peak boundary velocity gives $\tilde{U}_1 (v/\tilde{d}) = U_1 (v/d)$, which implies $\tilde{U}_1 = U_1 \tilde{d}/d = U_1(1 - \tilde{\eta})/(1 - \eta)$. For the $U_1 = 8000$, inferred from the experiment with $\eta = 0.97$ and used in most calculations, this gives $\tilde{U}_1 \approx 3.4 \times 10^4$ at $\eta = 0.874$ and $\tilde{U}_1 \approx 5.3 \times 10^4$ at $\eta = 0.8$. These are the peak values for $Re_o(t)$ for the experiment, and while they are achievable, it is perhaps not usual to be examining linear stability at such large Reynolds numbers.

Another practical difficulty for the case of large β is that, even if the rolls were present, they only occupy a small fraction of the depth that scales like $1/\beta$. This would lead to only a small contrast for traditional visualisation techniques using crystalline platelets.

A final question is the source of perturbations necessary to excite the instability. Endplates for the cylinders naturally break axial independence of the flow. They may lead to Ekman vortices, and can aid the formation of azimuthally aligned Taylor-vortex rolls. There is no obvious counterpart to break the axisymmetry of the flow. If the instability can only be excited from very low level disturbances, in combination with the start-stop being only a transient flow, it is quite possible that in many situations it would not reach sufficient amplitude to be observed.

For the future, with laser-based techniques such as particle image velocimetry (PIV) now more prevalent, such diagnostics may aid further experiments, and possibly lead to more frequent unexpected observations, of this instability over a wider range of radius ratios. Artificial perturbations, such as axially aligned grooves may also enhance the instability, possibly pushing it into regimes where Taylor or Görtler rolls would otherwise take over.

Funding. This research received no specific grant from any funding agency, commercial or not-for-profit sectors.

Declaration of interests. The authors report no conflict of interest.

REFERENCES

- ANDERECK, C DAVID, LIU, SS & SWINNEY, HARRY L 1986 Flow regimes in a circular couette system with independently rotating cylinders. *Journal of fluid mechanics* **164**, 155–183.
- BLONDEAUX, PAOLO & VITTORI, GIOVANNA 2021 Revisiting the momentary stability analysis of the stokes boundary layer. *Journal of Fluid Mechanics* **919**, A36.
- BURIN, M.J. & CZARNOCKI, C.J 2012 Subcritical transition and spiral turbulence in circular couette flow. *Journal of Fluid Mechanics* **709** (1), 106–122.
- COLES, DONALD 1965 Transition in circular couette flow. *Journal of Fluid Mechanics* **21** (3), 385–425.
- ERN, PATRICIA & WESFREID, JOSE EDUARDO 1999 Flow between time-periodically co-rotating cylinders. *Journal of Fluid Mechanics* **397**, 73–98.
- KOHUTH, KERRY RANDALL & NEITZEL, GP 1988 Experiments on the stability of an impulsively-initiated circular couette flow. *Experiments in fluids* **6** (3), 199–208.
- LOPEZ, JUAN M & MARQUES, FRANCISCO 2011 Instabilities and inertial waves generated in a librating cylinder. *Journal of fluid mechanics* **687**, 171–193.
- MARQUES, FRANCISCO & LOPEZ, JUAN M 1997 Taylor–couette flow with axial oscillations of the inner cylinder: Floquet analysis of the basic flow. *Journal of Fluid Mechanics* **348**, 153–175.
- NEITZEL, GP, KIRKCONNELL, CS & LITTLE, LJ 1995 Transient, nonaxisymmetric modes in the instability of unsteady circular couette flow. laboratory and numerical experiments. *Physics of Fluids* **7** (2), 324–334.
- NOIR, J, CALKINS, MA, LASBLEIS, M, CANTWELL, J & AURNOU, JM 2010 Experimental study of libration-driven zonal flows in a straight cylinder. *Physics of the Earth and Planetary Interiors* **182** (1–2), 98–106.
- OSTILLA-MÓNICO, RODOLFO, ZHU, XIAOJUE, SPANDAN, VAMSI, VERZICCO, ROBERTO & LOHSE, DETLEF 2017 Life stages of wall-bounded decay of taylor-couette turbulence. *Physical Review Fluids* **2** (11), 114601.
- SINGH, HARMINDER & PRIGENT, ARNAUD 2021 Turbulence generation and decay in the taylor–couette system due to an abrupt stoppage. *Journal of Fluid Mechanics* **918**, A21.
- TAYLOR, GEOFFREY INGRAM 1923 Viii. stability of a viscous liquid contained between two rotating cylinders. *Philosophical Transactions of the Royal Society of London. Series A, Containing Papers of a Mathematical or Physical Character* **223** (605–615), 289–343.
- VERSCHOOF, RUBEN A, HUISMAN, SANDER G, VAN DER VEEN, ROELAND CA, SUN, CHAO & LOHSE, DETLEF 2016 Self-similar decay of high reynolds number taylor-couette turbulence. *Physical review fluids* **1** (6), 062402.
- VERSCHOOF, RUBEN A, TE NIJENHUIS, ARNE K, HUISMAN, SANDER G, SUN, CHAO & LOHSE, DETLEF 2018 Periodically driven taylor–couette turbulence. *Journal of Fluid Mechanics* **846**, 834–845.
- VON KERCZEK, CHRISTIAN & DAVIS, STEPHEN H 1974 Linear stability theory of oscillatory stokes layers. *Journal of Fluid Mechanics* **62** (4), 753–773.
- WILLIS, ASHLEY P 2017 The openpipeflow navier–stokes solver. *SoftwareX* **6**, 124–127.
- YOUND, ANTHONY J, WILLIS, ASHLEY P & BARENGHI, CARLO F 2003 Reversing and non-reversing modulated taylor–couette flow. *Journal of Fluid Mechanics* **487**, 367–376.